



Research article

Sympathetic nerve infiltration promotes stomach adenocarcinoma progression via norepinephrine/ β 2-adrenoceptor/YKL-40 signaling pathwayYue-Hong Qi^{a,b,1}, Lu-Zi Yang^{a,1}, Lan Zhou^a, Li-Juan Gao^a, Jia-Yi Hou^a, Zi Yan^a, Xiao-Gang Bi^b, Cai-Ping Yan^c, De-Ping Wang^{a,**}, Ji-Min Cao^{a,*}^a Key Laboratory of Cellular Physiology at Shanxi Medical University, Ministry of Education, And the Department of Physiology, Shanxi Medical University, Taiyuan, China^b Department of Anesthesiology, Shanxi Provincial Peoples Hospital, Taiyuan, China^c Center of Translational Medicine, Shanxi Medical University, Taiyuan, China

ARTICLE INFO

Keywords:

Sympathetic nerve
Catecholamine
 β -adrenoceptor
YKL-40
Gastric cancer

ABSTRACT

Objective: This study aimed to address the status, role, and mechanism of sympathetic nerve infiltration in the progression of stomach adenocarcinoma (STAD).**Methods:** Sympathetic nerve and its neurotransmitter NE, β -ARs, and associated signaling molecules in the STAD tissues and the adjacent tissues from 46 STAD patients were examined using immunostaining, HPLC, and western blotting. The effects and mechanisms of β 2-AR activation on the proliferation, migration and invasion of AGS and SGC-7901 gastric cancer (GC) cell lines were examined using CCK-8, transwell, and western blotting assays. Correlations between genes and STAD survival were analyzed using bioinformatics.**Results:** Striking sympathetic nerve infiltration, elevations of NGF, TrkA, GAP43, TH, S100, NE, β 2-AR, YKL-40, syndecan-1, MMP9, CD206, and CD31 were observed in the STAD tissues compared to the adjacent tissues. Activation of β 2-AR in the two GC cell lines significantly amplified the expressions of NGF, YKL-40, MMP9, syndecan-1, p-STAT3 and p-ERK, and increased GC cell proliferation, migration and invasion. Bioinformatic analyses revealed positive correlations of NGF, β 2-AR, syndecan-1, and macrophage infiltration, respectively, with low survival of STAD, of β 2-AR respectively with STAT3, ERK1/2 (MAPK1/3), YKL-40, MMP9, and syndecan-1, and of YKL-40 with MMP9.**Conclusion:** Sympathetic nerves significantly infiltrated into human STAD tissues as a result of high NGF and TrkA expressions; elevated NE led to overactivation of β 2-AR-STAT3/ERK-YKL-40 signaling pathway, and finally caused cancer cell growth and invasion, M2 macrophage infiltration, angiogenesis, matrix degradation and STAD metastasis and progression.

1. Introduction

Stomach adenocarcinoma (STAD) is the most common and lethal carcinoma in human digestive system. Approximately 97% of the gastric cancer (GC) cases are adenocarcinomas. The exact pathogenesis of STAD is largely unknown, although unhealthy foods, infection of *helicobacter pylori*, and genetics are considered the pathogenic factors [1, 2].

YKL-40, also known as chitinase-3-like protein 1 (CHI3L1), is a member of the mammalian chitinase-like proteins (CLPs) belonging to the glycoside hydrolase family 18. These CLPs are expressed in multiple cell types including malignant tumor cells and inflammatory cells. The

focus of CLPs in cancer research is YKL-40 [3]. YKL-40 is a secreted glycoprotein and is involved in innate immune and extracellular matrix remodeling. There is a clear correlation between circulating YKL-40 levels and poor prognosis in lung, breast, liver, prostate, bladder, colon, and other types of cancers. Patients with metastatic breast carcinoma had significantly higher serum YKL40 levels than controls [4, 5]. YKL40 is not only a tumor biomarker but also functions as a key factor in the development, invasion, metastasis, and treatment resistance of cancers [6]. However, YKL40 studies in GC are still rare, only few literatures can be found currently in the PubMed, respectively reporting serum YKL-40 levels [7] and YKL-40 overexpression in GC patients [8]. Most of

* Corresponding author.

** Corresponding author.

E-mail addresses: wangdeping@sxmu.edu.cn (D.-P. Wang), caojimin@sxmu.edu.cn (J.-M. Cao).¹ These authors contributed equally to this work.

the knowledges about the carcinogenic role of YKL-40 are from other cancers which cannot be simply translated to GC. Therefore, it is still necessary to understand the role of YKL40 in GC.

The values of β -adrenoceptors (β -ARs) blockers in cancer treatment have been emphasized in recent years [9], especially the β 2-AR blockers, because β 2-AR is widely expressed in human GC tissues compared to other types of β -ARs [10]. However, a research work that orchestrates sympathetic nerve infiltration (SNI), transmitter norepinephrine (NE)/catecholamines, β 2-AR, and YKL-40 in GC progression is still lacking.

Autonomic nerve infiltration into cancer mass was reported to be associated with the development of a variety of tumors [11–14]. Indeed, vagal nerve has been suggested to play an important role in the pathogenesis of GC [11]. However, the role of sympathetic nerve in GC has rarely been investigated. It is still unknown whether sympathetic nerve infiltrates into the GC tissues and promotes GC progression due to molecular entities discussed above. The present study was, therefore, set to investigate the role of sympathetic nerve infiltration (SNI) on STAD malignancy with a series of approaches including experimental studies on human STAD tissues and GC cell lines, and bioinformatics analyses. We demonstrated the presence, characteristics, effects, and potential mechanisms of SNI in STAD, and established a novel signaling pathway by which SNI promoted STAD progression, and in which, YKL-40 was likely a key downstream effector. We also demonstrated significant correlations between adrenergic signaling and STAD survival.

2. Materials and methods

2.1. Patients and tumor tissues

After institutional ethics approval by Shanxi Provincial Peoples Hospital, Taiyuan, China, and obtaining informed written consent forms from patients, 46 patients (21 males and 25 females, 66.0 ± 4.8 years old) diagnosed with STAD were recruited for this study. The STAD tissues and adjacent non-tumor gastric mucosal and submucosal tissues (>5 cm laterally from the edge of tumor region) were harvested during radical tumor excision surgeries under routine anesthesia. Half of the tissue samples were immediately frozen in liquid nitrogen and stored at -80°C for western blotting assays and the other half of the tissue samples were fixed overnight in 10% phosphate-buffered formalin for immunohistochemical (IHC) and immunofluorescent (IF) staining. Formalin-fixed tissue samples were dehydrated with graded alcohol, hyalinized with xylene, and then imbedded in paraffin. Tissue blocks were cut into 5 μm sections and mounted on slides. Some STAD tissue blocks were cut into 10- μm sections for IF staining of tyrosine hydroxylase (TH) aiming to better show the fiber-like structure of the infiltrated sympathetic nerves.

2.2. Immunohistochemistry

Tissue sections were deparaffinized in xylene and rehydrated with graded alcohol and water. Endogenous peroxidase was blocked by incubation with solution A (endogenous peroxidase blocker, Zhongshan Golden bridge Biotechnology, China) for 30 min. Antigen retrieval was performed by boiling the tissue slides in EDTA antigen repair solution (pH 8.0) (Zhongshan Golden Bridge Biotechnology (ZSGB-BIO), Beijing, China) in a water bath ($92\text{--}98^\circ\text{C}$) for 20 min. Tissue sections were rinsed three times in phosphate buffer solution (PBS) and then were incubated overnight at 4°C with primary antibodies (all from Abcam, England) respectively against the following antigens: NGF, dilution 1:2000; TrkA, 1:100; GAP43, 1:800; TH, 1:30; S100, 1:2000; YKL40, 1:1000; CD206, 1:1000; syndecan-1, 1:1000; MMP9, 1:500; CD31, 1:100; β 1-AR, 1:100; β 2-AR, 1:100; β 3-AR, 1:100). The sections were then washed with PBS for thrice and incubated with solution B (reaction enhancer) (Zhongshan Golden Bridge Biotechnology, China) for 30 min at room temperature. Subsequently, tissue sections were incubated with the peroxidase (enhancer enzyme)-conjugated goat anti-rabbit/mouse secondary antibody solution (ZSGB-BIO, Beijing, China) for 60 min at room

temperature. Target proteins were visualized with DAB chromogen (Dako REALTM EnVision™ detection system). Tissue sections were counterstained with hematoxylin and cover-slipped with neutral balsam. Positive signals were taken under a microscope. Three fields were examined in each section, and paired sections (STAD and adjacent) were checked for each selected patient. The positively stained areas in each field were calculated using ImageJ software [15].

2.3. Immunofluorescent staining

Immunofluorescent (IF) staining of TH was performed in 10- μm STAD tissue sections aiming to better show the fiber-like structure of the infiltrated sympathetic nerves. The procedures of IF staining were basically the same as IHC staining, except that the tissue sections were treated with Triton X-100 and goat serum, but not treated with endogenous peroxidase blocker (H_2O_2), and a fluorescent goat anti-rabbit secondary antibody against TH (dilution 1:200) (ZSGB-BIO, Beijing, China) was used. After staining, tissue sections were cover-slipped with DAPI. Images were taken under a fluorescent microscope. The areas of the positive fluorescent signals in each field were calculated using ImageJ software [16].

2.4. Western blotting

The primary antibodies against TH, NGF, TrkA, YKL-40, CD31, syndecan-1, and MMP9 were purchased from Abcam (Cambridgeshire, England). The primary antibodies of STAT3, p-STAT3, ERK, and p-ERK were purchased from Cell Signaling Technology (Boston, USA). Total proteins were extracted using radio immunoprecipitation assay lysis buffer and quantified using the BCA assay kit (Solarbio Science & Technology Co., Beijing, China). To perform western blotting, total proteins of 40 μg from each sample were electrophoresed on 10% SDS-PAGE and were electrically transferred (300 mA for 3 h) onto the nitrocellulose membranes using Bio-Rad Mini-PROTEAN Tetra according to the standard protocol. The nitrocellulose membranes were then blocked with TBS containing 5% nonfat milk and 0.1% Tween-20 at room temperature for 2 h. Subsequently, the membranes were incubated with the primary antibodies respectively against NGF, TrkA, GAP43, TH, S100, YKL-40, CD206, syndecan-1, MMP-9, CD31, STAT3, p-STAT3, ERK, p-ERK, and GAPDH at 4°C for overnight. The dilutions for these primary antibodies were all 1:1000. After washing thrice with TBST buffer, the membranes were incubated with the peroxidase-conjugated secondary antibody against rabbit or mouse IgG (dilution 1:10,000) corresponding to the primary antibodies. Positive fluorescent signals were visualized with electrochemiluminescence (ECL) agent (Solarbio Science & Technology Co., Beijing, China) according to the manufacturer's instructions. Analysis of the grey intensity was performed using ImageJ software. STAD and adjacent tissue samples were collected from at least three patients [17].

2.5. High performance liquid chromatography-electrochemical detection (HPLC-ED)

HPLC-ED was used to detect the levels of sympathetic neurotransmitter NE in the STAD tissues and the adjacent tissues [18]. To prepare the NE standard solution for HPLC chromatograms, NE powder (Sigma, USA) was dissolved in ultrapure water to achieve a NE stock solution of 10^{-3} mol/L, and 0.1 mol/L acetic acid (10%) was added to the solution and then stored at -20°C to prevent NE oxidative denaturation. The NE solution was diluted to a working concentration (10^{-7} mol/L) before HPLC-ED. Freshly harvested STAD tissues (0.183 g) and adjacent tissues (0.183 g) were respectively homogenized in 200 μL buffer containing (in mmol/L) 147 NaCl, 4 KCl, 2.3 CaCl_2 and 1.2 MgCl_2 (pH 7.4), and then the homogenates were centrifuged at 26,916 g for 15 min at 4°C to remove any residues. The supernatant of each sample was diluted with 600 μL diluent buffer, then was treated with 20 μL of 10% acetic acid (to stabilize NE) and filtered with 0.2- μm Millipore. HPLC-ED was performed using a LC-20A liquid

chromatograph equipped with a LC-20AT solvent delivery unit and an electrochemical detector (ED723, GL-Sciences, Kyoto, Japan). A laboratory solution workstation software (Shimadzu, Kyoto, Japan) was used for data acquisition. Chromatographic separations were carried out on a Shim-pack GIST C18 column (250 mm × 4.6 mm, 5 μm particle size, Shimadzu, Kyoto, Japan). The mobile phase consisted of (in mmol/L) 30 KH₂PO₄, 0.05 EDTA, and 0.32 sodium 1-octane sulfonate (SOS) in 400 mL ultrapure water (pH adjusted to 4.0 with phosphoric acid). Then the mobile phase solution was mixed with 44 mL of 10% methanol and filtered with a 0.22-μm filter membrane and was degassed. The detection voltage of the ED723 detector was set to 750 mV (Diamond electrode). The flow rate was 1 mL/min and the injection volume were 5 μL. The column temperature was kept at 30 °C. The HPLC-ED analyses were performed on the STAD tissues and adjacent tissues from three patients.

2.6. Gastric cancer cell lines and cell culture

Human AGS and SGC-7901 gastric cancer cell lines were purchased from Shanghai Institutes for Biological Sciences, Chinese Academy of Sciences (Shanghai, China). AGS and SGC-7901 cells were respectively cultured in Ham's F-12 medium (Hyclone, USA) and phenol red-free RPMI-1640 medium supplemented with 10% fetal bovine serum (FBS) (Biological Industries (BI), Israel) and 1% penicillin-streptomycin-glutamine (100×) solution (Biological Industries (BI), Israel). Cultures were kept in a humidified incubator with 5% CO₂ at 37 °C. Cells were then treated with 10 μmol/L isoproterenol (ISO) (a β-AR agonist) (Sigma, USA) or ISO + ICI118,551 (25 μmol/L) (a selective β₂-AR antagonist) for indicated time points [19].

2.7. Cell proliferation assay

Proliferations of AGS and SGC-7901 cells were determined using CCK-8 kit (Kumamoto, Japan). Cell concentration was adjusted to 3 × 10⁴ cells/mL. Cells were then seeded into 96-well plates with 100 μL culture media in each well and cultured for overnight. Isoprenaline (ISO) (10 μmol/L) or ISO + ICI118,551 (25 μmol/L) was added to the culture medium at the beginning of culture. After culture for 24 h, the medium was removed and cells were washed twice with phosphate-buffered solution (PBS), and were cultured in 100 μL fresh medium containing 10 μL CCK-8 reagent for an additional 1 h. The optical density (OD) value reflecting proliferation was measured at the wavelength 450 nm using a microplate reader [20].

2.8. Cell migration assay

The AGS and SGC-7901 cells (2.5 × 10⁴ cells) in 100 μL serum-free medium were planted into the upper chamber of a transwell with 8-μm pores (Corning, NY, USA). The bottom chamber was filled with 700 μL medium supplemented with 10% FBS and ISO (10 μmol/L) or ISO + ICI118,551 (25 μmol/L). After 12 h of incubation, non-migratory cells were removed gently with a cotton swab, and the migrated cells were stained with crystal violet for 30 min then fixed with 4% paraformaldehyde for 30 min. The numbers of migrated cells were counted in 6 random fields (200× magnification). The assay was repeated three times, and each assay was performed in triplicate [21].

2.9. Matrigel cell invasion assay

GC cell invasion assay was performed using a transwell with 8-μm pores (Corning, NY, USA). Matrigel matrix aliquot was taken out from -80 °C freezer and thawed on ice at 4 °C for overnight, then was swirled to ensure that the material was evenly dispersed and kept chilled on wet ice. Matrigel matrix was diluted with serum-free cold medium to a final concentration of 0.3 mg/mL. In a hood, a sterile pipet was used to gently add 0.1 mL diluted matrigel matrix to each of the 24 wells in the 8-μm pore transwell insert. The 24-well plates with coated transwell inserts were incubated at 37 °C for at least 1 h. The remaining liquids were

carefully removed from the transwell inserts without disturbing the layer of matrigel. Cell treatment and invasion assay were then performed similarly as the migration assay [21].

2.10. Bioinformatic analysis

We used UALCAN, an interactive web resource (<http://ualcan.path.uab.edu/index.html>) which provides cancer OMICS data, including TCGA (The Cancer Genome Atlas) [22] and MET500 database [23], to screen the top 50 overexpressed genes and to analyze the expression of YKL-40 (CHI3L1) in STAD patients. TIMER (Tumor Immune Estimation Resource) [24] (<https://cistrome.shinyapps.io/timer>) provides survival module between gene expression and clinical outcome in a multivariable Cox proportional hazard model, and has the functions to draw Spearman's correlation curves and to provide pair-wise gene expression correlation analysis for given sets of TCGA and/or GTEx (the Genotype-Tissue Expression) database [25]. Using TIMER, we performed the correlation analysis between ADRB genes (ADRB1, ADRB2, and ADRB3) and CHI3L1, and analyzed the correlations of NGF expression and macrophage infiltration with the cumulative survival rate. GEPIA (the Gene Expression Profiling Interactive Analysis) [26] (<http://gepia.cancer-pku.cn/index.html>) is a newly developed interactive web server for analyzing the RNA sequencing expression data which cover 9,736 tumors and 8,587 normal samples from the TCGA and the GTEx projects. Based on multiple genes, GEPIA provides these analyses: multiple gene comparison, correlation analysis, and dimensionality reduction. We analyzed the disease-free survival (ADRB1, ADRB2, and ADRB3) and overall survival (SDC1) based on Cox PH Model with GEPIA. Meanwhile, a series of correlation analyses were carried out about pair-wise genes (CHI3L1 and MMP9, CHI3L1 and SDC1, CHI3L1 and STAT3, and CHI3L1 and MAPK).

2.11. Statistical analysis

Statistical Product and Service Solutions 17.0 was used to perform statistical analysis. All data were expressed as mean ± standard deviation (SD). Difference comparison among multiple groups were performed using analysis of variance (ANOVA) followed by a post hoc test. Comparison between two groups were analyzed with grouped *t* test. The relationship between YKL-40 expression and patient survival time was analyzed by Kaplan-Meier analysis. Spearman correlation analysis was used to evaluate the correlation between pair-wise genes and to calculate Spearman's rank correlation coefficient (R). Frequencies of categorical variables were compared using the Chi-squared test. A *P* value less than 0.05 was considered statistically significant.

3. Results

3.1. Significant sympathetic nerve infiltration in the STAD tissue and its association with tumor metastasis and prognosis

Immunohistochemical (IHC) stains of thin (5 μm) gastric tissue sections showed high expressions of nerve growth factor (NGF) and its high-affinity receptor tropomyosin receptor kinase A (TrkA) in the interstitial areas of STAD tissues compared to the adjacent tissues (Figure 1A). S100, a Schwann cell marker of nerve myelin sheath which guides axon growth, growth associated protein 43 (GAP43), a nerve growth cone marker reflecting sympathetic nerve sprouting, and tyrosine hydroxylase (TH), a sympathetic nerve marker, were all highly expressed in the interstitial areas of STAD tissues compared to the adjacent tissues (Figure 1A, B). The positive stains of the above five proteins (NGF, TrkA, S100, GAP43, and TH) basically showed dotted structures in 5-um sections, which might reflect the varicose structures of the sympathetic nerve terminals. In order to show the "fiber-like" structure of the infiltrated sympathetic nerves, we performed the IHC and immunofluorescent (IF) staining of TH in thick (10 μm) STAD tissue sections, and results showed that the sympathetic nerve fibers were mainly distributed in the interstitial areas

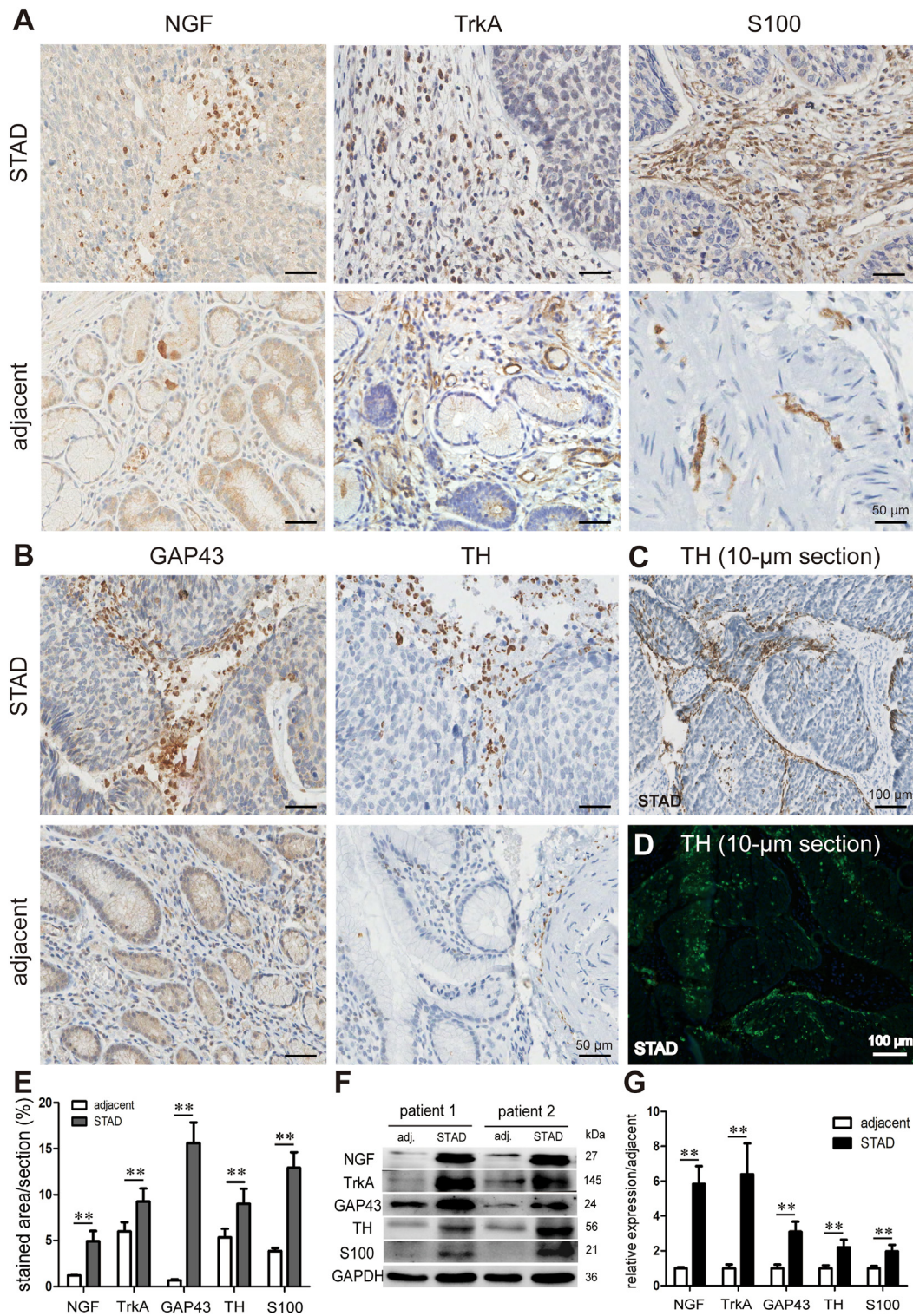


Figure 1. Amplified expressions of sympathetic nerve infiltration-associated proteins in the STAD tissue compared to the adjacent tissue. (A) Immunohistochemical (IHC) stains (brown) of NGF, TrkA, and S100 in 5-um sections. (B) IHC stains of GAP43 and TH (brown) in 5-um sections. (C) IHC stain of TH (brown) in 10-um section of the STAD tissue. (D) Immunofluorescent (IF) stain of TH (green) in 10-um section of the STAD tissue. Note that both IHC and IF stains of TH in thick (10 μm) STAD tissue sections showed “fiber-like” structures of sympathetic nerves with high density near the tumor nests which suggested serious sympathetic nerve infiltration. (E) Semiquantitative analysis of the IHC stains in 5-μm sections. N = 3 sections/patient. *P < 0.05, **P < 0.01. (F) Representative Western blots of NGF, TrkA, GAP43, TH, and S100 in the STAD tissue and adjacent (adj.) tissue. (G) Statistical results of Western blots. **P < 0.01, n = 3 independent experiments.

closing to the STAD nests (Figure 1 C, D). Semiquantitative analysis of the IHC stains in 5-μm sections showed that these five proteins associated with SNI (NGF, TrkA, S100, GAP43, and TH) were significantly higher in the STAD tissues than in the adjacent tissues (Figure 1 E).

We also performed western blotting to check the protein expression levels of NGF, TrkA, GAP43, TH, and S100, and results showed that the expression levels of these five proteins were all significantly higher in the STAD tissues than in the adjacent tissues (Figure 1 F, G).

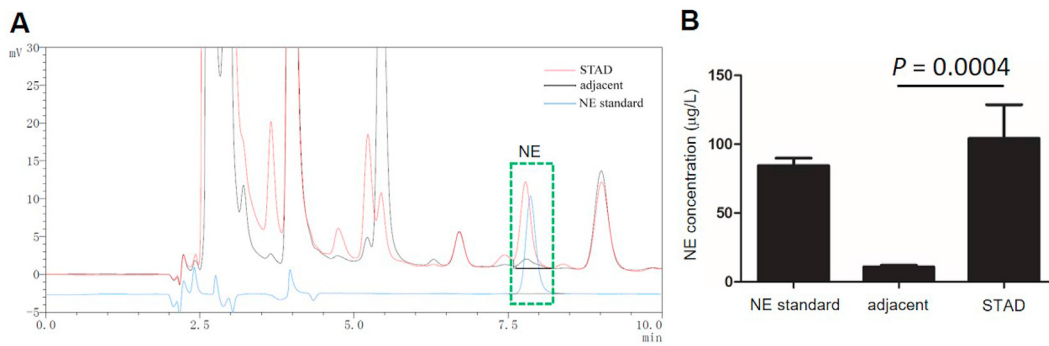


Figure 2. HPLC-ED results of NE levels in the STAD and the adjacent tissues. (A) Representative HPLC-ED recording of NE in the homogenates of STAD and adjacent tissues, which showed high NE level in the STAD tissue compared to the adjacent tissue. The NE peak of the homogenates and the NE standard was marked by a green square. (B) Statistical results of HPLC-ED, n = 4 independent experiments.

To further investigate the association of SNI with STAD metastasis and prognosis, patients with available clinicopathological features and complete follow-up data was excavated. The 46 human STAD tissue samples were divided to two groups (with or without SNI) according to the immunostaining presence of sympathetic nerve invasion. Correlation analysis revealed that SNI in STAD tissues was significantly correlated with tumor invasion depth ($P < 0.05$), lymph node metastasis ($P < 0.05$), and clinical TNM stages ($P < 0.01$) (Table S1).

3.2. Elevation of sympathetic neurotransmitter norepinephrine and amplified β -adrenoceptor expression in the STAD tissue

To identify whether the infiltrated sympathetic nerves were functionally active and could release its transmitter norepinephrine (NE), we

performed HPLC-ED to detect the NE levels in the homogenate supernatants of both STAD tissues and adjacent tissues. NE standard curve was established to calibrate the tissue NE level (Figure S1). The regression equation of NE standard was $(R)f(x) = 1792.63 * x + 101.86$, and the correlation coefficient (R) = 0.9999825. HPLC-ED results showed that the NE level was much higher in the STAD tissues ($86.13 \pm 12.10 \mu\text{g/L}$) than in the adjacent tissues ($10.75 \pm 1.19 \mu\text{g/L}$) ($P = 0.0004$) (Figure 2).

Because NE exerts its effect mainly via the β -adrenoceptors (β -ARs) in tumors, we further examined the expressions of β -ARs in the gastric tissues using IHC staining. Results showed that β 1-AR was basically negative in the STAD tissue and the adjacent tissue; β 2-AR was strongly expressed in the STAD tissue compared to the adjacent tissue; while β 3-AR was slightly but significantly higher in the STAD tissue than in the adjacent tissue (Figure 3).

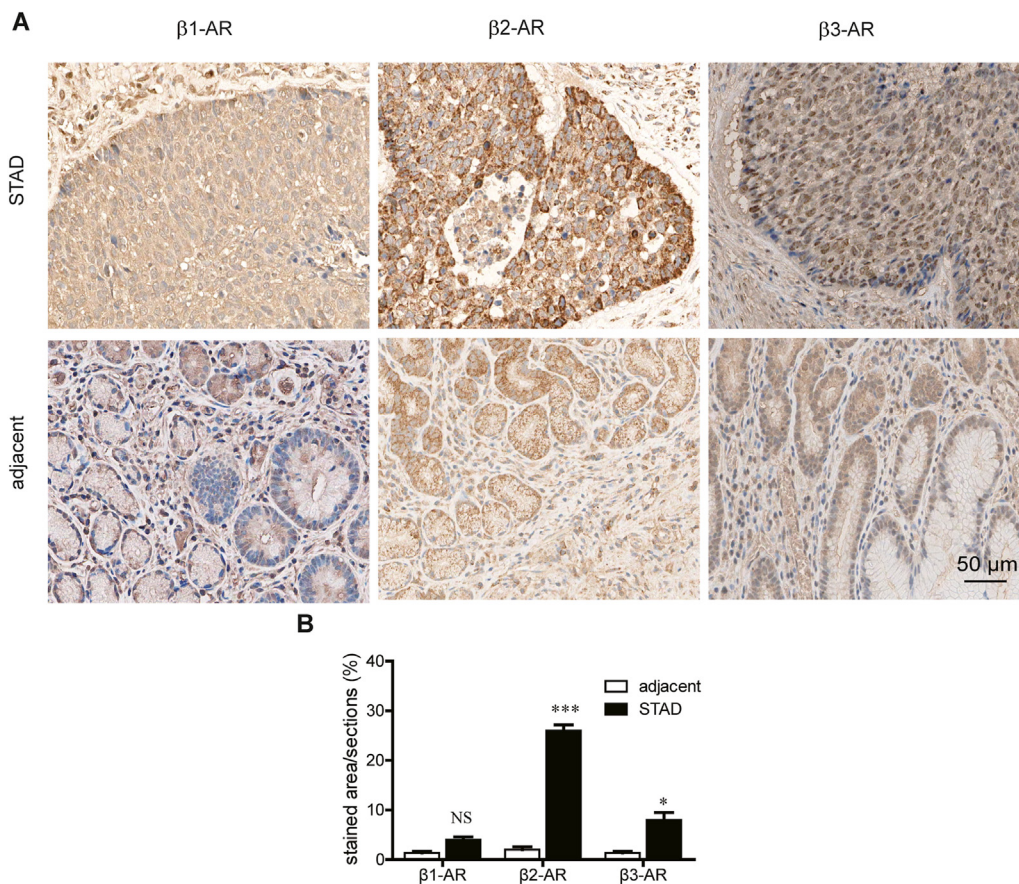


Figure 3. IHC stains of β 1-AR, β 2-AR, and β 3-AR in the STAD and adjacent tissues (5- μm sections). (A) Representative IHC image. Note that β 1-AR was basically negative in the STAD tissue and adjacent tissue. β 2-AR was strongly expressed in the STAD tissue compared to the adjacent tissue. β 3-AR positive signal was found weakly present in the STAD tissue but was negative in the adjacent tissue. Scale bar, 50 μm . (B) Semiquantitative analysis of the positive IHC signals of β 1-AR, β 2-AR, and β 3-AR in the STAD tissue and adjacent tissue. * $P < 0.05$, ** $P < 0.01$, n = 3 sections/patient. Scale bar, 50 μm .

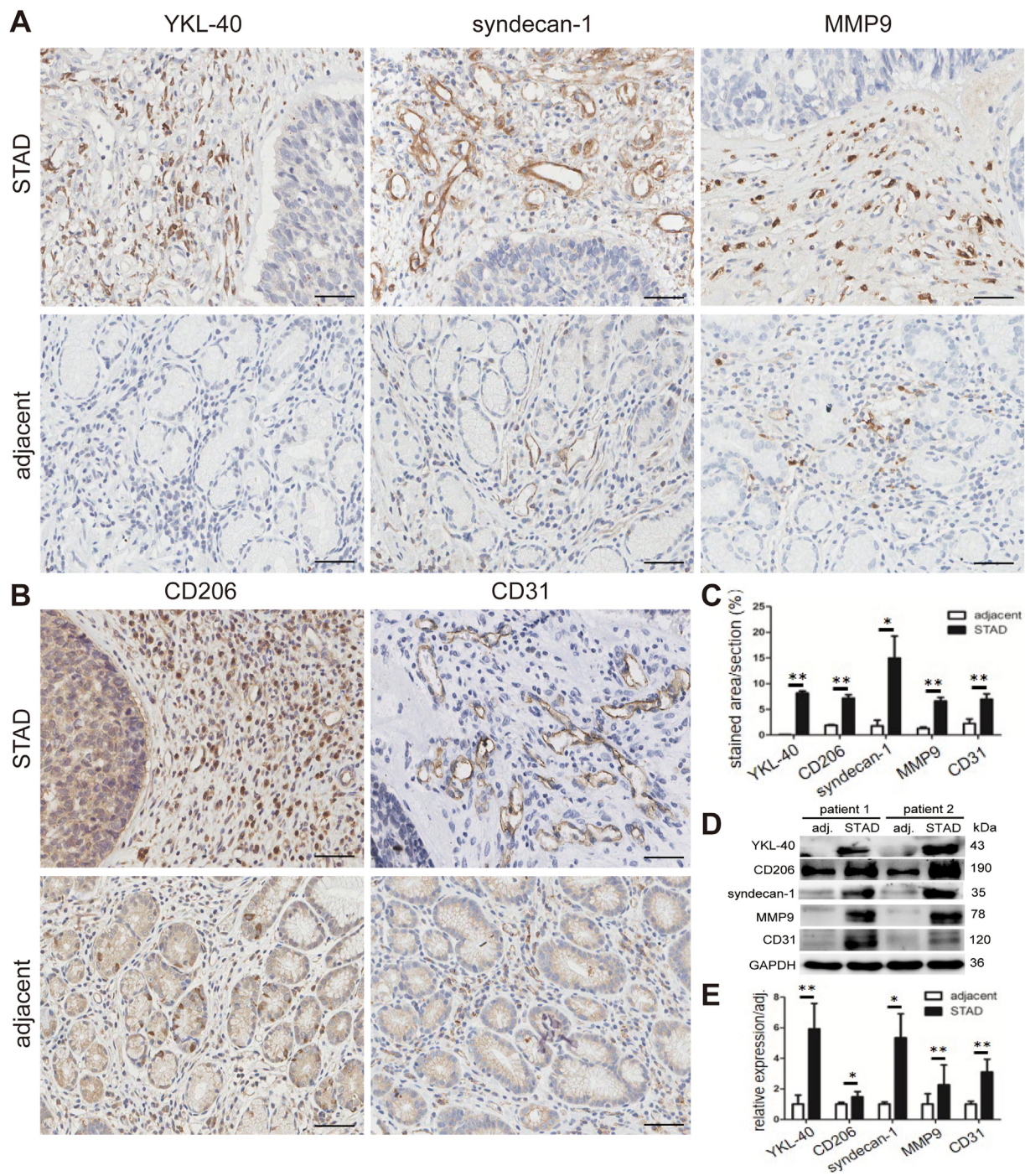


Figure 4. High expressions of YKL-40, syndecan-1, MMP9, CD206, and CD31 in the STAD tissue compared to the adjacent tissue. (A) Representative IHC stain of YKL-40, syndecan-1, and MMP9 (brown). Scale bar, 50 μ m. (B) Representative IHC stain of CD206 and CD31 (brown). (C) Semiquantitative analysis of the positive IHC stains of the above five proteins. * $P < 0.05$, ** $P < 0.01$, $n = 3$ sections/patient. Scale bar, 50 μ m. (D) Representative Western blots of the above five proteins. (E) Statistical results of WB. * $P < 0.05$, ** $P < 0.01$, $n = 3$ independent experiments.

3.3. High expressions of YKL-40, CD206, syndecan-1, MMP9, and CD31 in the STAD tissues

IHC stains showed amplified amounts of YKL-40, CD206, syndecan-1, MMP9, and CD31 in the STAD tissues compared to the adjacent tissues (Figure 4A, B, C). The positive stains of YKL-40, CD206, and MMP9 exhibited dotted structures, while syndecan-1 and CD31 were visible mainly in the small blood vessel walls in the interstitial areas between STAD nests (Figure 4A, B). Western blotting assays confirmed the high

expressions of YKL-40, CD206, syndecan-1, MMP9, and CD31 in the STAD tissues compared to the adjacent tissues (Figure 4D, E). High expression of CD206 (a marker of M2 macrophage) indicated increased M2 macrophage infiltration. Syndecan-1 is a cell surface heparan sulfate proteoglycan and is involved in tumor cell differentiation and metastasis, thus elevated syndecan-1 might worsen STAD prognosis. Elevated MMP9 means magnified matrix degradation which favors STAD cell metastasis. CD31 is a marker of endothelium and its elevation suggests increased angiogenesis in the STAD tissues which also supports the blood supply for STAD.

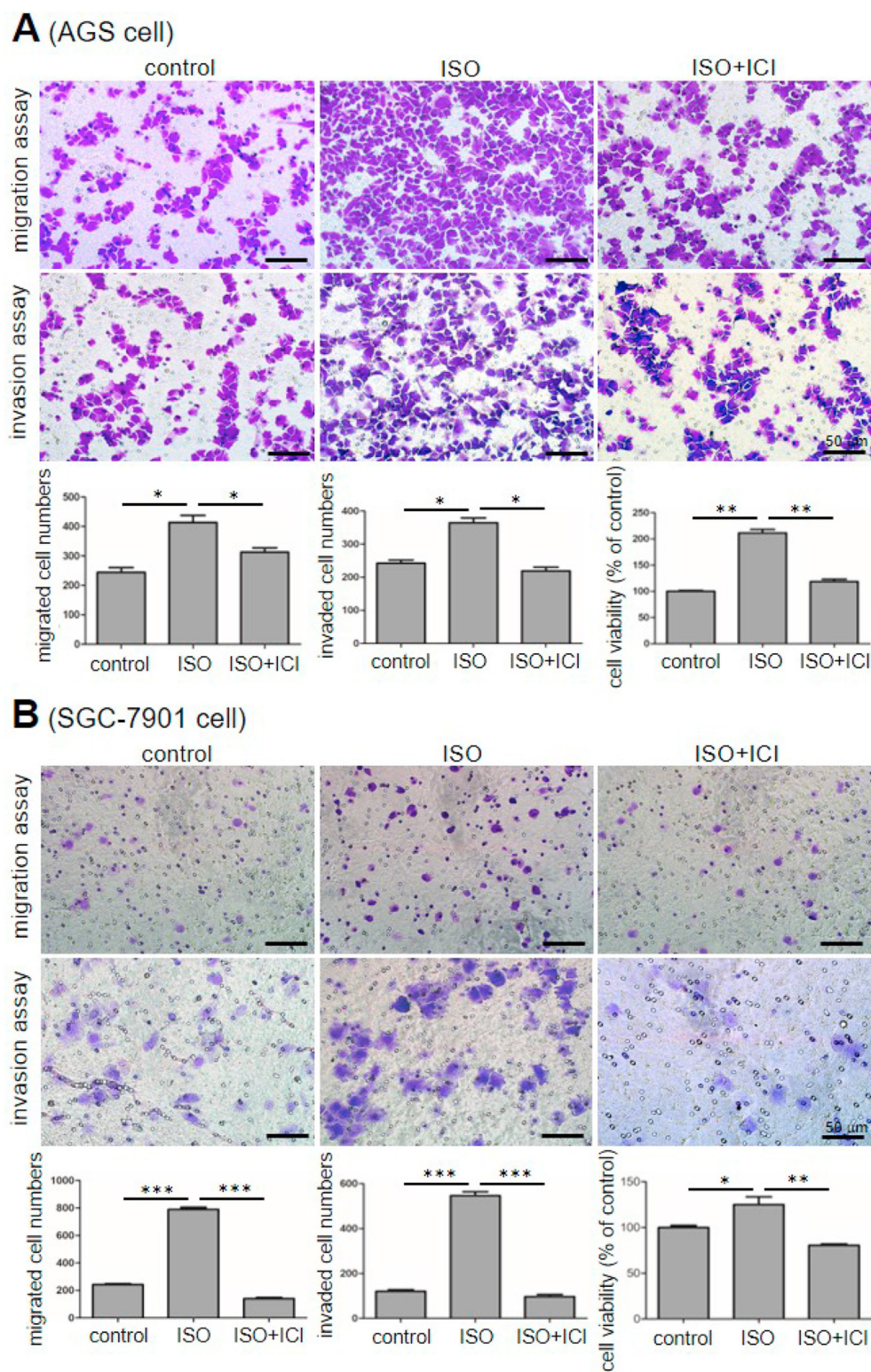


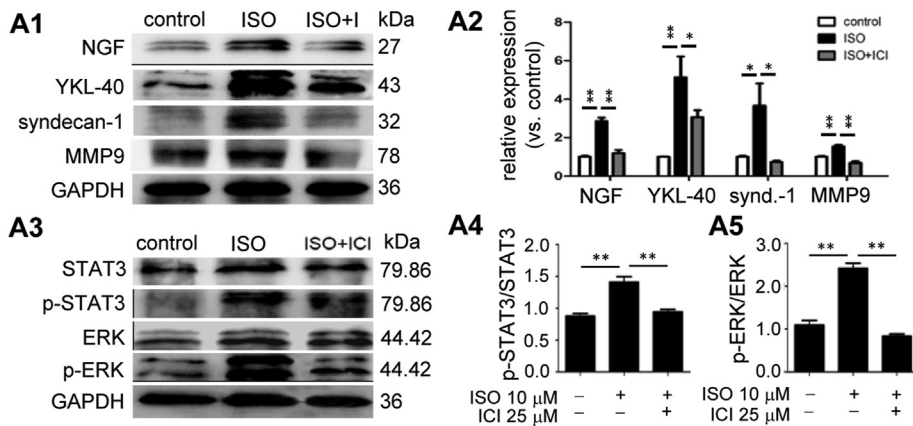
Figure 5. Effects of isoprenaline on the proliferation, migration, and the invasion of AGS and SGC-7901 cell lines examined by CCK8, transwell, and matrigel assay. (A) AGS cells. Upper row, representative images of cell migration assays. Middle row, images of AGS cell invasion assays. Scale bar, 50 μ m. Lower row, statistical results of cell migration, invasion, and proliferation/viability assays. * $P < 0.05$, ** $P < 0.01$, $n = 3$ independent experiments. (B) SGC-7901 cells. Upper row, representative images of cell migration assay. Middle row, images of cell invasion assay. Scale bar, 50 μ m. Lower row, statistical results of cell migration, invasion, and viability assays. Note that isoprenaline (ISO) (10 μ mol/L) significantly increased the migration, invasion, and viability of both cell lines, while blocking β 2-AR with ICI118,551 (ICI) (25 μ mol/L) abolished these effects of ISO in both cell lines. * $P < 0.05$, ** $P < 0.01$, *** $P < 0.001$, $n = 3$ independent experiments.

3.4. Activation of β 2-AR enhanced the proliferation, migration, and invasion of GC cells *in vitro*

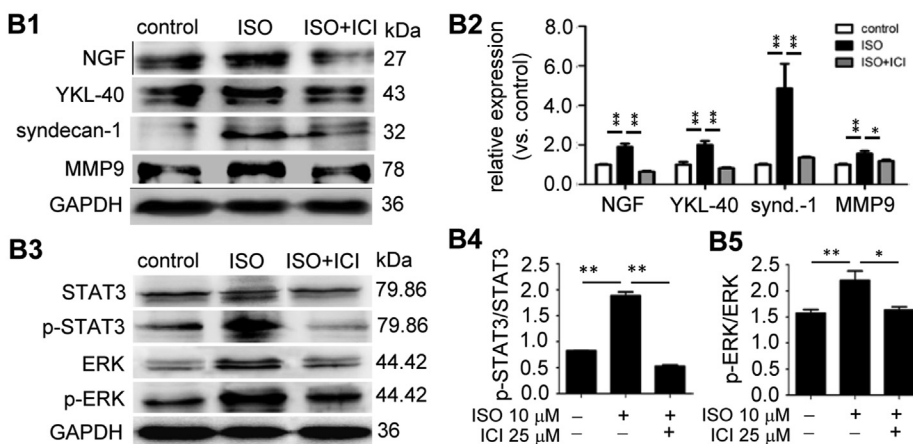
Above IHC stains exhibited upregulation of adrenergic signaling in the STAD tissues. Using AGS and SGC-7901 GC cell lines, we further identified whether activation of β -ARs would enhance the proliferation, migration, and invasion of GC cells. Results showed that activation of

β -ARs with ISO (a non-selective agonist of β -ARs) significantly increased the viability, migration, and invasion of AGS cells (Figure 5A) and SGC-7901 cells (Figure 5B) compared with cells not exposed to ISO. Selective blockade of β 2-AR with ICI118,551 abolished the above effects of ISO both in AGS cells (Figure 5A) and SGC-7901 cells (Figure 5B), suggesting that the above effects of ISO were leadingly mediated by β 2-AR.

A (AGS cell)



B (SGC-7901 cell)



3.5. Upregulations of NGF/YKL-40/syndecan-1/MMP9 expression and STAT3/ERK phosphorylation in response to β2-AR activation in GC cell lines in vitro

Above tissue studies demonstrated SNI (indicated by TH), magnified adrenergic signaling (NE and β2-AR), increased M2 macrophage (marked by CD206), angiogenesis (CD31), matrix degradation (MMP9), and cancer metastasis (YKL-40 and syndecan-1) in STAD tissues. Using western blotting of two GC cell lines, we further studied whether GC cells could express NGF, syndecan-1, YKL-40, and MMP9, and identified the phosphorylation of the key kinases (STAT3 and ERK) in response to β-ARs activation. Results showed that ISO (10 μmol/L) increased the expressions of NGF, syndecan-1, YKL-40, and MMP9 in AGS cells (Figure 6A1, A2) and SGC-7901 cells (Figure 6B1, B2), and increased the phosphorylation of STAT3 and ERK in both AGS cells (Figure 6A3, A4, A5) and SGC-7901 cells (Figure 6B3, B4, B5). Selective blockade of β2-AR with ICI118,551 (25 μmol/L) abolished these effects of ISO in both cell lines (Figure 6A, B), suggesting that GC cells is a source of NGF that stimulates sympathetic nerve sprouting and infiltration, and GC cells can respond to the transmitter NE or catecholamines resulting in activation of the β2-AR/PKA/STAT3/ERK/YKL-40 signaling, and consequently the GC cells proliferate, migrate, and invade, and finally lead to tumor metastasis.

3.6. Correlations of sympathetic nerve infiltration and β2-AR with the survival of STAD revealed by bioinformatic analysis

We accessed the UALCAN, downloaded the OMICS data (TCGA and MET500) of STAD, and built the heat maps of the top 50 overexpressed

Figure 6. Effects of isoprenaline on the protein expressions of NGF, YKL-40, syndecan-1, MMP9, STAT3, and ERK in AGS and SGC-7901 cell lines examined by Western blotting. (A) AGS cells. (A1) Representative WB of NGF, YKL-40, syndecan-1, and MMP9. (A2) Statistical WB results of the four proteins shown in A1. **P* < 0.05, ***P* < 0.01, n = 3 independent experiments. (A3) Representative WB of STAT3, p-STAT3, ERK, and p-ERK. (A4) p-STAT3/STAT3 ratio. ***P* < 0.01, n = 3. (A5) p-ERK/ERK ratio. ***P* < 0.01. (B) SGC-7901 cells. (B1) Representative WB of NGF, YKL-40, syndecan-1, and MMP9. (B2) Statistical WB results of the four proteins shown in B1. **P* < 0.05, ***P* < 0.01, n = 3. (B3) Representative WB of STAT3, p-STAT3, ERK, and p-ERK. (B4) p-STAT3/STAT3 ratio. ***P* < 0.01. (B5) p-ERK/ERK ratio. **P* < 0.05, ***P* < 0.01, n = 3.

genes (Figure S2), which showed that YKL-40 (CHI3L1) was the 28th highly expressed gene in human STAD. YKL-40 was overexpressed in all the tumor stages of STAD (*P* < 0.05), especially in the grade 1 (Figure 7A). High expression of NGF was significantly correlated with low overall survival of STAD (*P* = 0.0084) (Figure 7B). High macrophage infiltration was significantly correlated with the cumulative overall survival of STAD (*P* = 0.004) (Figure 7C). High expression of β2-AR (*P* = 0.021), but not β1-AR (*P* = 0.73) or β3-AR (*P* = 0.63), was significantly correlated with low disease-free survival of STAD (Figure 7D, E, F), and was also weakly correlated with high YKL-40 level (Figure 7G, H, I). High level of YKL-40 was significantly correlated with high levels of STAT3 (*P* = 4.9e-37), MAPK1 (ERK2) (*P* = 1.9e-26), and MAPK3 (ERK1) (*P* = 1.4e-19) in STAD (Figure 7J, K, L). In addition, high YKL-40 was significantly correlated with high MMP9 level (*P* = 6.5e-79) (Figure 7M) and high syndecan-1 (SDC1) level (*P* = 3.2e-21) (Figure 7N). High syndecan-1 was significantly correlated with the overall survival of STAD (*P* = 0.032) (Figure 7O). By performing genetic association analyses, we further demonstrated that high expression of β2-AR was positively correlated with GATA3 (*P* = 0.000) but was negatively correlated with TP53 (*P* = 4.02e-03) (Figure S3), suggesting the roles of GATA3 and TP53 in NE/β2-AR signaling-mediated STAD progression.

4. Discussion

Identification of the molecular basis of the sympathetic nerve activity in the progression of STAD is crucial for further study of anti-tumor treatment. Here, we identified significant SNI, NE elevation, and upregulation of β2-AR and YKL-40 levels in the STAD tissues. We further showed that high β2-AR expression was significantly correlated with a

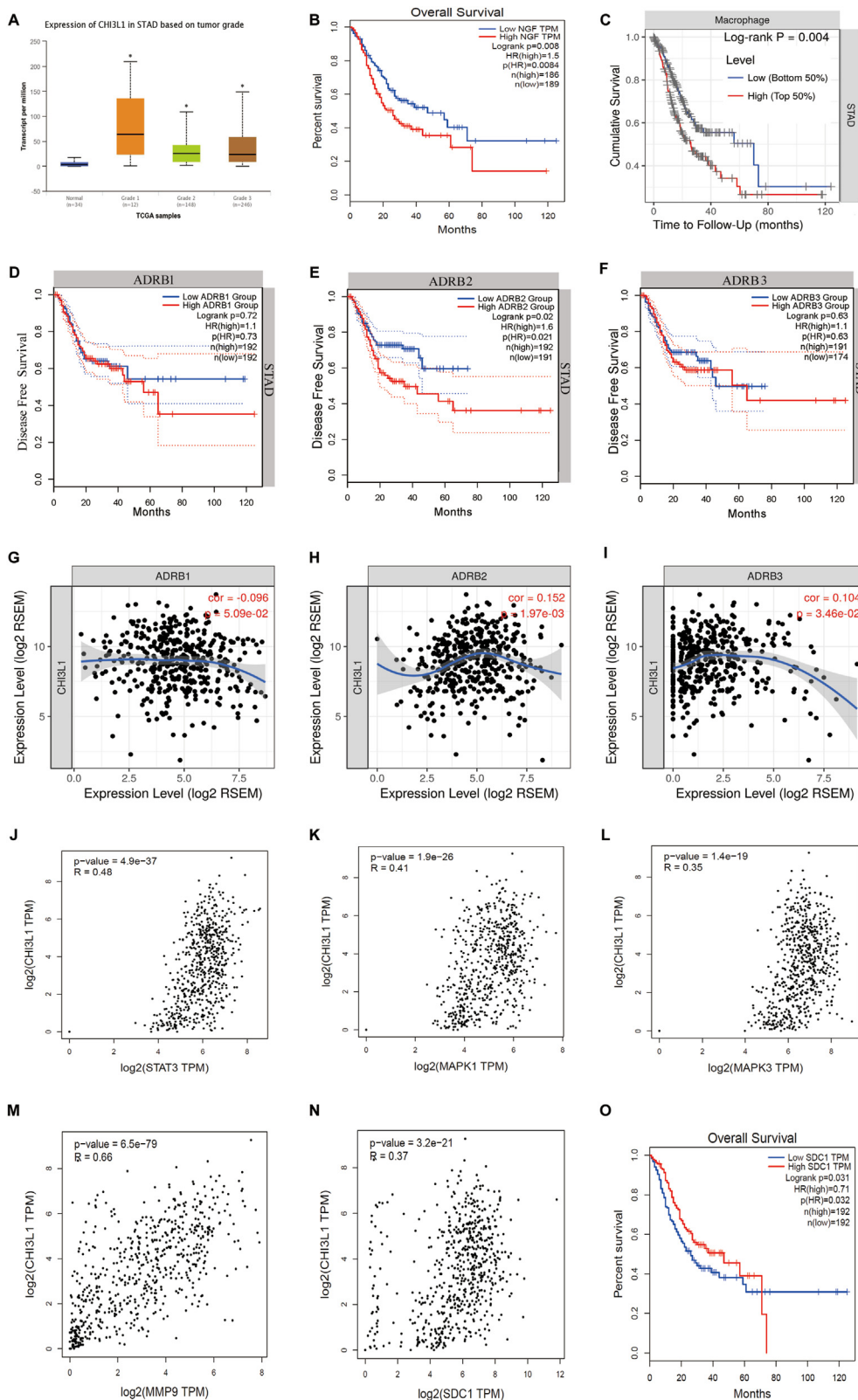


Figure 7. Bioinformatic analyses on the correlations among gene expression levels and survivals in STAD patients. (A) Expression levels of YKL-40 (CHI3L1) in STAD patients with different tumor grades. Note that YKL-40 was overexpressed in all the tumor stages of STAD, especially in grade 1, compared to normal subjects. *P < 0.05 vs. normal. (B) High expression of NGF was significantly correlated with low overall survival in STAD (P = 0.0084). (C) High macrophage infiltration was significantly correlated with low cumulative survival in STAD (P = 0.004). (D, E, F) Correlations of β 1-AR (ADRB1), β 2-AR (ADRB2), and β 3-AR (ADRB3) expression levels with disease free survival of STAD, respectively. β 2-AR (P = 0.021), but not β 1-AR (P = 0.73) or β 3-AR (P = 0.63), was significantly correlated with the disease-free survival. (G, H, I) Correlations of β 1-AR, β 2-AR, and β 3-AR expression levels with YKL-40 (CHI3L1) expression level in STAD, respectively. β 2-AR was weakly but positively correlated with YKL-40 (p = 0.00197, R = 0.152), while β 1-AR (P = 0.0509) and β 3-AR (P = 0.0346) were not significantly correlated with YKL-40. (J, K, L) Significant correlations of CHI3L1 expression level respectively with STAT3 (P = 4.9e-37, R = 0.48), MAPK1 (ERK2) (P = 1.9e-26, R = 0.41), and MAPK3 (ERK1) (P = 1.4e-19, R = 0.35) in STAD. (M, N) Significant correlations of CHI3L1 expression level with MMP9 (P = 6.5e-79, R = 0.66) and SDC1 (syndecan-1) (P = 3.2e-21, R = 0.37) expressions, respectively. (O) Significant correlation of syndecan-1 (SDC1) with the overall survival of STAD (P = 0.032).

poor perceived prognosis of STAD. Elevated YKL-40 interacted with syndecan-1 and enhanced the expression of MMP9, and finally together led to extracellular matrix disintegration, macrophage infiltration, and angiogenesis facilitating STAD progression. We also showed that selective activation of β 2-AR promoted M2 macrophage infiltration, matrix degradation, angiogenesis, and GC cell metastasis.

Emerging evidence suggests that sympathetic nervous system acts as a crucial part of cancer microenvironment and contributes to the growth and progression of multiple tumors[27-30]. Sympathetic nerve may affect the tumor by releasing NE which activates β -ARs especially the β 2-AR expressed in the target cancer cells [10, 31]. Catecholamines, including NE, interact directly with tumor cells, and promote NGF

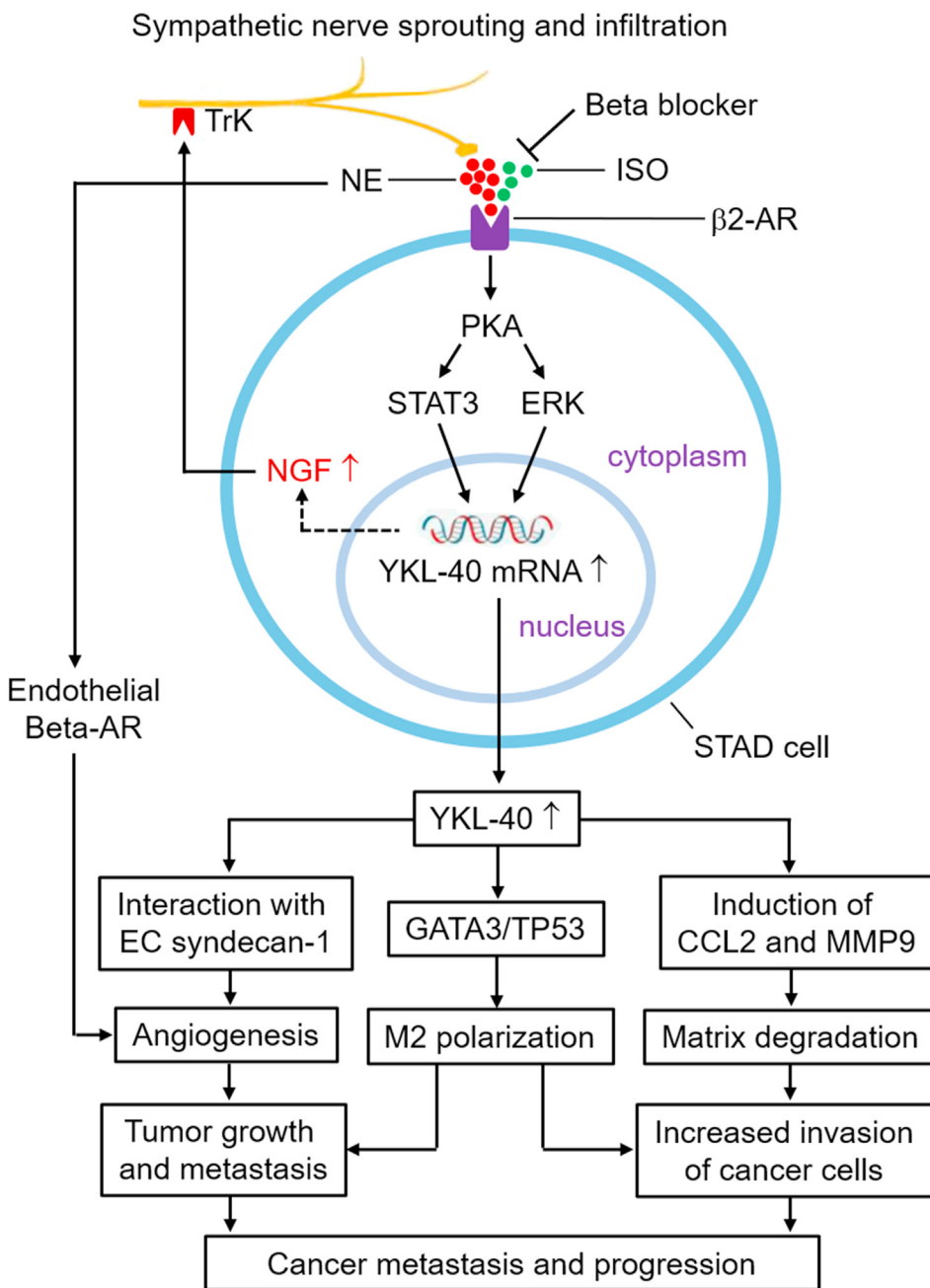


Figure 8. Proposed signaling pathways by which sympathetic nerve infiltration induces STAD metastasis and progression. Briefly, NGF is highly expressed in STAD cells and is secreted into tumor microenvironment and promotes sympathetic nerve sprouting and infiltration into the interstitial areas of STAD tissues by activating TrkA in the nerve; sympathetic nerve terminals release NE and thus activates the β2-AR/cAMP/PKA pathway of STAD cells; PKA phosphorylates STAT3 and ERK; p-ERK and p-STAT3 acting as transcription factors enter the nucleus and promote the transcription of YKL-40 in STAD cells; secreted YKL-40 interacts with endothelial syndecan-1 and enhances angiogenesis, tumor growth and metastasis, and induces MMP9 expression and thus leads to matrix degradation facilitating tumor cell invasion and metastasis. YKL-40 may also affect GATA3 and/or TP53 to induce M2 macrophage polarization and thus cancer cell invasion. In addition, NE can directly induce tumor angiogenesis via β-ARs in the endothelial cells. Beta blockers, especially the β2-AR blocker, may switch off this signaling chain at the upstream site and thus inhibit STAD progression.

secretion, pancreatic hyperinnervation, and β2-AR-dependent development of pancreatic ductal adenocarcinoma in a feedforward fashion [31]. Generally, sympathetic nerve ingrowth into the cancerous tissues may be established through the following signaling: NGF production → NGF receptors (TrkA, etc.) → sympathetic nerve sprouting and infiltration. Previous study reported that the NGF-TrkA axis contributed to the progression of head and neck squamous cell carcinoma [32]. Once SNI is built, it may affect tumor cells via the following signaling: NE release → β2-AR → Gs protein → cAMP → PKA → downstream signaling → tumor cell proliferation, migration, and metastasis [33]. Nevertheless, the present study demonstrated that amplified adrenergic signaling is a dominant part of the STAD microenvironment. We for the first time demonstrated a very high NE level in the STAD tissue compared to the adjacent tissue using HPLC-ED. This novel result suggests that the infiltrated sympathetic nerves in the STAD tissue are functionally active in releasing its transmitter. We also demonstrated high expression of β2-AR,

and a mild elevation of β3-AR, but no change of β1-AR, in the STAD tissues. These findings suggest that STAD cells are highly capable to respond to NE (or other kinds of catecholamines) using the β2-AR signaling pathway and potentially also the β3-AR pathway to a mild degree. In vitro studies confirmed that selective activation of β2-AR stimulated the expression of NGF and promoted GC cell proliferation, migration, and invasion, further supporting the importance of SNI/NE/β2-AR axis in STAD progression.

YKL-40 has been correlated with mal-prognosis of advanced human cancers. YKL-40 induces the coupling of syndecan-1 and αvβ3 integrin in human microvascular endothelial cells and enhances angiogenesis in vitro and in vivo [34]. YKL-40 enhances tumor angiogenesis via interacting with syndecan-1 in endothelial cells and promotes cancer cell metastasis via stimulating the secretions of pro-inflammatory and pro-invasive factors MMP9, CCL2 and CXCL2 [35,36]. Taking the advantage of large-scale OMICS data of STAD, we performed

bioinformatic analyses on the correlations among the expression levels of YKL-40 and β -adrenergic signaling molecules and the prognosis of STAD. Results revealed that β 2-AR (but not β 1-AR and β 3-AR) was positively correlated with YKL-40 and with low overall survival of STAD. High YKL-40 in STAD significantly correlated with high NGF, macrophage infiltration, low overall survival, and low cumulative survival. Collectively, our study indicated that catecholamines activated the β 2-AR signaling and thus increased the levels of YKL-40 in GC cells, and demonstrated the key role of YKL-40 in the molecular basis of angiogenesis and GC metastasis both in vitro and in vivo, as blockade of β 2-AR inhibited YKL-40 expression and migration and invasion of GC. Except for upregulating YKL-40 expression, NE can directly induce angiogenesis via beta receptors on endothelial cells [37]. Therefore, SNI can induce tumor angiogenesis via both the NE and YKL-40 pathways, this interplay may further enhance tumor angiogenesis resulting in progression of GC.

We further investigated the downstream signaling of β 2-AR activation in GC cells which is still unclear. It is known that β 2-AR belongs to the family of G protein coupled receptors. Activation of β 2-AR triggers the Gs/AC (adenylate cyclase)/cAMP/PKA signaling cascade in some cancer cells [27, 33]. The following signal transductions after activation of PKA are usually complicated and heterogenous in variant cancer cells, for example, CREB, NF κ B, and AP-1 in pancreatic cancer cells [33], STAT3 [38] and STAT3/MicroRNA373³⁹ in GC cells. Our bioinformatic analysis showed that YKL-40 was positively associated with STAT3, ERK, MMP9, and syndecan-1, and syndecan-1 was correlated with low overall survival of STAD. In addition, we demonstrated pharmacologically that β 2-AR activation upregulated the phosphorylated (activated) forms of STAT3 and ERK in two GC cell lines (shown in Figure 6). These results are consistent with previous reports [38, 39] and suggest that p-STAT3 and p-ERK are involved in STAD progression. It is known that STAT3 and ERK are both transcription factors after phosphorylation. The p-STAT3 forms dimers, translocate from cytoplasm into the nucleus and then bind to DNA and induce transcription of its downstream target genes [40]. ERK belongs to the mitogen-activated protein kinase (MAPK) family [41] and can also promote the transcription of target genes after entering the nucleus. There have been studies indicating that both p-STAT3 and p-ERK can promote the transcription of YKL-40 [42,43]. We showed here that β 2-AR activation increased the levels of p-STAT3, p-ERK, and YKL-40. These results suggest the importance of STAT3/ERK-YKL-40 axis in STAD progression.

The complex tumor microenvironment is shaped by cells entering it. Inflammatory cells in tumor microenvironment may play a crucial role in helping the tumor growth and invasion. Bioinformatic databases of tumors, including TCGA database, can help to evaluate the complex interaction of immune cells in the tumor microenvironment of cancer. Tumor-associated macrophages (TAMs) exert an immunosuppressive effect in the tumor microenvironment and enhance tumor growth, angiogenesis, and metastasis. Moreover, GATA3 regulates the polarization of macrophages and the interactions between TAMs and cancer cells [44, 45, 46, 47]. Polarized M2 macrophages dominate the TAMs and promote tumor progression, while M1 macrophages usually suppress tumor progression [47, 48]. Our bioinformatic analysis revealed that the density of TAMs was associated with a poor prognosis of STAD. TP53 acts as a potential regulator of M2 macrophage polarization and promotes macrophage infiltration in STAD patients [49]. β -adrenergic stimulation induces macrophage polarity towards the M2 side in the M1-M2 spectrum [50]. To further explore the potential regulatory function of β 2-AR in M2 macrophage polarization in STAD, we analyzed all available data from TIMER (a web server for comprehensive analysis of tumor-infiltrating immune cells using TCGA database). Results showed the enrichment of adrenergic signaling molecules in the microenvironment of STAD, suggesting that β 2-AR signaling may play an important role in the development of STAD via YKL-40, GATA3 and TP53 induced M2 macrophage polarization and TAMs infiltration [51]. These results suggest the importance of TCGA data analysis in demonstrating the complex interaction of immune cells in the tumor microenvironment.

In summary, the present study demonstrates dramatic SNI in the STAD tissue resulted from high expression of NGF by the tumor cells; infiltrated sympathetic nerves release NE which in turn activates β 2-AR and the downstream signaling including STAT3, ERK, YKL-40, and potentially also GATA3 and TP53. YKL-40 interacts with syndecan-1 and enhanced MMP9 expression and finally together lead to extracellular matrix disintegration, macrophage infiltration, and angiogenesis facilitating STAD progression. The study also highlighted the usefulness and importance of tumor bioinformatic databases as tools in evaluating the complex interaction of immune cells in the tumor microenvironment of cancer. A summary of the conceived signaling pathway is shown in Figure 8. The study suggests the therapeutic value of blocking SNI and/or β 2-AR signaling in STAD.

Limitations. The study has some limitations. First, the patient cohort is relatively smaller, this may restrict the accuracy of certain evaluations, such as the relationship between lymph node invasion and survival. The use of online databases helped us to evaluate the relationships. Second, we did not differentiate the NPY-positive (innervating blood vessels) and NPY-negative (innervating gastroenteric ganglia) sympathetic nerves by immunohistochemical staining, this may affect the recognition on which type of sympathetic nerves innervates the tumor.

Declarations

Author contribution statement

Yue-Hong Qi: Conceived and designed the experiments; Performed the experiments; Analyzed and interpreted the data; Contributed reagents, materials, analysis tools or data; Wrote the paper.

Lu-Zi Yang; Lan Zhou; Jia-Yi Hou; Zi Yan: Performed the experiments. Li-Juan Gao; Cai-Ping Yan: Analyzed and interpreted the data.

Xiao-Gang Bi: Contributed reagents, materials, analysis tools or data.

De-Ping Wang: Conceived and designed the experiments; Performed the experiments; Wrote the paper.

Ji-min Cao: Conceived and designed the experiments; Wrote the paper.

Funding statement

Zi Yan was supported by Applied Basic Research Program of Shanxi Province [201901D211320], Returned Overseas Researchers of Shanxi Province [2020-081]. Prof Ji-min Cao was supported by National Natural Science Foundation of China [82170523]. This work was supported by Key Medical Science and Technology Program of Shanxi Province [2020XM01], Shanxi "1331 Project" Quality and Efficiency Improvement Plan [1331KFC].

Data availability statement

Data will be made available on request.

Declaration of interest's statement

The authors declare no competing interests.

Additional information

Supplementary content related to this article has been published online at <https://doi.org/10.1016/j.heliyon.2022.e12468>.

References

- [1] H. Brenner, D. Rothenbacher, V. Arndt, *Epidemiology of stomach cancer*, *Methods Mol. Biol.* 472 (2009) 467–477.
- [2] G. Moradi, K. Karimi, N. Esmailnasab, D. Roshani, *Survival of patients with stomach cancer and its determinants in Kurdistan*, *Asian Pac. J. Cancer Prev. APJCP* 17 (2016) 3243–3248.

- [3] A.P. Bussink, D. Spejjer, J.M. Aerts, R.G. Boot, Evolution of mammalian chitinase-like members of family 18 glycosyl hydrolases, *Genetics* 177 (2007) 959–970.
- [4] A. Rusak, K. Jabloniska, P. Dziegiel, The role of YKL-40 in a cancerous process, *Postepy Hig. Med. Dosw.* 70 (2016) 1286–1299.
- [5] B.V. Jensen, J.S. Johansen, P.A. Price, High levels of serum HER-2/neu and YKL-40 independently reflect aggressiveness of metastatic breast cancer, *Clin. Cancer Res.* 9 (2003) 4423–4434.
- [6] K. Hermunen, L.M. Soveri, M.K. Boisen, H.K. Mustonen, C. Dehrendorf, C.H. Haglund, et al., Postoperative serum CA19-9, YKL-40, CRP and IL-6 in combination with CEA as prognostic markers for recurrence and survival in colorectal cancer, *Acta Oncol.* 59 (2020) 1416–1423.
- [7] V. Itik, O. Kemik, A. Kemik, A.C. Dulger, A. Sümer, Y.U. Soyoral, et al., Serum YKL-40 levels in patients with gastric cancer, *Biomarkers Cancer* 3 (2011) 25–30.
- [8] J. Bi, S.H. Lau, Z.L. Lv, D. Xie, W. Li, Y.R. Lai, et al., Overexpression of YKL-40 is an independent prognostic marker in gastric cancer, *Hum. Pathol.* 40 (2009) 1790–1797.
- [9] M. Koh, T. Takahashi, Y. Kurokawa, T. Kobayashi, T. Saito, T. Ishida, et al., Propranolol suppresses gastric cancer cell growth by regulating proliferation and apoptosis, *Gastric Cancer* 24 (2021) 1037–1049.
- [10] T. Shan, X. Cui, W. Li, W. Lin, Y. Li, X. Chen, et al., Novel regulatory program for norepinephrine-induced epithelial-mesenchymal transition in gastric adenocarcinoma cell lines, *Cancer Sci.* 105 (2014) 847–856.
- [11] C.M. Zhao, Y. Hayakawa, Y. Kodama, S. Muthupalani, C.B. Westphalen, G.T. Andersen, et al., Denervation suppresses gastric tumorigenesis, *Sci. Transl. Med.* 6 (2014) 250ra115.
- [12] Y. Xia, Y. Wei, Z.Y. Li, X.Y. Cai, L.L. Zhang, X.R. Dong, et al., Catecholamines contribute to the neovascularization of lung cancer via tumor-associated macrophages, *Brain Behav. Immun.* 81 (2019) 111–121.
- [13] E.V. Yang, A.K. Sood, M. Chen, Y. Li, T.D. Eubank, C.B. Marsh, et al., Norepinephrine up-regulates the expression of vascular endothelial growth factor, matrix metalloproteinase (MMP)-2, and MMP-9 in nasopharyngeal carcinoma tumor cells, *Cancer Res.* 66 (2016) 10357–10364.
- [14] A. Eckerling, I. Ricon-Becker, L. Sorski, E. Sandbank, S. Ben-Eliyahu, Stress and cancer: mechanisms, significance and future directions, *Nat. Rev. Cancer* 21 (2021) 767–785.
- [15] J.S. Duerr, *Immunohistochemistry*. WormBook, 2006, pp. 1–61.
- [16] D. Robertson, K. Savage, J.S. Reis-Filho, C.M. Isacke, Multiple immunofluorescence labelling of formalin-fixed paraffin-embedded (FFPE) tissue, *BMC Cell Biol.* 9 (2008) 13.
- [17] B.T. Kurien, R.H. Scofield, Western blotting: an introduction, *Methods Mol. Biol.* 1312 (2015) 17–30.
- [18] S.K. Tschirner, F. Gutzki, E.H. Schneider, R. Seifert, V. Kaever, Neurotransmitter and their metabolite concentrations in different areas of the HPRT knockout mouse brain, *J. Neurol. Sci.* 365 (2016) 169–174.
- [19] B. Wei, X. Sun, Z. Geng, M. Shi, Z. Chen, L. Chen, et al., Isoproterenol regulates CD44 expression in gastric cancer cells through STAT3/MicroRNA373 cascade, *Biomaterials* 105 (2016) 89–101.
- [20] A. Adan, Y. Kiraz, Y. Baran, Cell proliferation and cytotoxicity assays, *Curr. Pharmaceut. Biotechnol.* 17 (2016) 1213–1221.
- [21] J. Marshall, Transwell[®] invasion assays, *Methods Mol. Biol.* 769 (2011) 97–110.
- [22] C. Li, M. Wang, J. Wei, W. Zhang, H. Liu, D. Zhao, Construction of a pyroptosis-related genes signature to improve the prognostic prediction and therapeutic drugs selection in patients with pancreatic cancer, *Int. J. Gen. Med.* 15 (2022) 6387–6403.
- [23] D.R. Robinson, Y.M. Wu, R.J. Lonigro, P. Vats, E. Cobain, J. Everett, et al., Integrative clinical genomics of metastatic cancer, *Nature* 548 (2017) 297–303.
- [24] S. Wang, L. Cheng, F. Jing, G. Li, Screening and identification of immune-related genes for immunotherapy and prognostic assessment in colorectal cancer patients, *BMC Med. Genom.* 15 (2022) 177.
- [25] Y. Li, S. Han, B. Wu, C. Zhong, Y. Shi, C. Lv, et al., CXCL11 correlates with immune infiltration and impacts patient immunotherapy efficacy: a pan-cancer analysis, *Front. Immunol.* 13 (2022), 951247.
- [26] Z. Tang, C. Li, B. Kang, G. Gao, C. Li, Z. Zhang, GEPIA: a web server for cancer and normal gene expression profiling and interactive analyses, *Nucleic Acids Res.* 45 (2017) W98–W102.
- [27] X. Zhi, B. Li, Z. Li, J. Zhang, J. Yu, L. Zhang, et al., Adrenergic modulation of AMPK-dependent autophagy by chronic stress enhances cell proliferation and survival in gastric cancer, *Int. J. Oncol.* 54 (2019) 1625–1638.
- [28] M. Hulsurkar, Z. Li, Y. Zhang, X. Li, D. Zheng, W. Li, Beta-adrenergic signaling promotes tumor angiogenesis and prostate cancer progression through HDAC2-mediated suppression of thrombospondin-1, *Oncogene* 36 (2017) 1525–1536.
- [29] N. Roda, G. Blandano, P.G. Pelicci, Blood vessels and peripheral nerves as key players in cancer progression and therapy resistance, *Cancers* 13 (2021) 4471.
- [30] A.H. Zahalka, P.S. Frenette, Nerves in cancer, *Nat. Rev. Cancer* 20 (2020) 143–157.
- [31] B.W. Renz, R. Takahashi, T. Tanaka, M. Macchini, Y. Hayakawa, Z. Dantes, et al., β 2 adrenergic-neurotrophin feedforward loop promotes pancreatic cancer, *Cancer Cell* 33 (2018) 75–90.
- [32] C. Lin, Z. Ren, X. Yang, R. Yang, Y. Chen, Z. Liu, et al., Nerve growth factor (NGF)-TrkA axis in head and neck squamous cell carcinoma triggers EMT and confers resistance to the EGFR inhibitor erlotinib, *Cancer Lett.* 472 (2020) 81–96.
- [33] D. Zhang, Q.Y. Ma, H.T. Hu, M. Zhang, β 2-adrenergic antagonists suppress pancreatic cancer cell invasion by inhibiting CREB, NF κ B and AP-1, *Cancer Biol. Ther.* 10 (2020) 19–29.
- [34] B. Geng, J. Pan, T. Zhao, J. Ji, C. Zhang, Y. Che, et al., Chitinase 3-like 1-CD44 interaction promotes metastasis and epithelial-to-mesenchymal transition through β -catenin/Erk/Akt signaling in gastric cancer, *J. Exp. Clin. Cancer Res.* 37 (2018) 208.
- [35] J. Kzhyshkowska, S. Yin, T. Liu, Y. Riabov, I. Mitrofanova, Role of chitinase-like proteins in cancer, *Biol. Chem.* 397 (2016) 231–247.
- [36] I.J. Yeo, C.K. Lee, S.B. Han, J. Yun, J.T. Hong, Roles of chitinase 3-like 1 in the development of cancer, neurodegenerative diseases, and inflammatory diseases, *Pharmacol. Ther.* 203 (2019), 107394.
- [37] H. Hondermarck, P. Jobling, The sympathetic nervous system drives tumor angiogenesis, *Trends Cancer* 4 (2) (2018) 93–94.
- [38] Y.J. Lu, Z.J. Geng, X.Y. Sun, Y.H. Li, X.B. Fu, X.Y. Zhao, et al., Isoprenaline induces epithelial-mesenchymal transition in gastric cancer cells, *Mol. Cell. Biochem.* 408 (2015) 1–13.
- [39] B. Wei, X. Sun, Z. Geng, M. Shi, Z. Chen, L. Chen, et al., Isoproterenol regulates CD44 expression in gastric cancer cells through STAT3/MicroRNA373 cascade, *Biomaterials* 105 (2016) 89–101.
- [40] M. Ashrafzadeh, A. Zarrabi, S. Oroui, V. Zarrin, E. Rahmani Moghadam, A. Zabolian, et al., STAT3 pathway in gastric cancer: signaling, therapeutic targeting and future prospects, *Biology* 9 (2020) 126.
- [41] S. Lee, J. Rauch, W. Kolch, Targeting MAPK Signaling in cancer: mechanisms of drug resistance and sensitivity, *Int. J. Mol. Sci.* 21 (2020) 1102.
- [42] J.T. Fan, Z.Y. Zhou, Y.L. Luo, Q. Luo, S.B. Chen, J.C. Zhao, et al., Exosomal lncRNA NEAT1 from cancer-associated fibroblasts facilitates endometrial cancer progression via miR-26a/b-5p-mediated STAT3/YKL-40 signaling pathway, *Neoplasia* 23 (2021) 692–703.
- [43] H. Tang, Y. Sun, Z. Shi, H. Huang, Z. Fang, J. Chen, et al., YKL-40 induces IL-8 expression from bronchial epithelium via MAPK (JNK and ERK) and NF- κ B pathways, causing bronchial smooth muscle proliferation and migration, *J. Immunol.* 190 (2013) 438–446.
- [44] V. Gambardella, J. Castillo, N. Tarazona, F. Gimeno-Valiente, C. Martínez-Ciarpaglini, M. Cabeza-Segura, et al., The role of tumor-associated macrophages in gastric cancer development and their potential as a therapeutic target, *Cancer Treat Rev.* 86 (2020), 102015.
- [45] H. Wang, T. Tian, J. Zhang, Tumor-associated macrophages (TAMs) in colorectal cancer (CRC): from mechanism to therapy and prognosis, *Int. J. Mol. Sci.* 22 (2021) 8470.
- [46] A.A. El-Arabey, M. Denizli, P. Kanlikilicler, R. Bayraktar, C. Ivan, M. Rashed, et al., GATA3 as a master regulator for interactions of tumor-associated macrophages with high-grade serous ovarian carcinoma, *Cell. Signal.* 68 (2020), 109539.
- [47] M.R. Riih a, P.A. Puolakkainen, Tumor-associated macrophages (TAMs) as biomarkers for gastric cancer: a review, *Chronic Dis. Transl. Med.* 4 (2018) 156–163.
- [48] M.A.F. Yahaya, M.A.M. Lila, S. Ismail, M. Zainol, N.A.R.N.M. Afizan, Tumour-associated macrophages (TAMs) in colon cancer and how to reeducate them, *J. Immunol. Res.* 2019 (2019), 2368249.
- [49] A.A. El-Arabey, M. Abdalla, A.R. Abd-Allah, SnapShot: TP53 status and macrophages infiltration in TCGA-analyzed tumors, *Int. Immunopharm.* 86 (2020), 106758.
- [50] D.M. Lamkin, H.Y. Ho, T.H. Ong, C.K. Kawanishi, V.L. Stoffers, N. Ahlawat, et al., β -Adrenergic-stimulated macrophages: comprehensive localization in the M1-M2 spectrum, *Brain Behav. Immun.* 57 (2016) 338–346.
- [51] M. Kawada, H. Seno, K. Kanda, Y. Nakanishi, R. Akitake, H. Komekado, et al., Chitinase 3-like 1 promotes macrophage recruitment and angiogenesis in colorectal cancer, *Oncogene* 31 (2012) 3111–3123.